

Controllable Human-Object Interaction Synthesis

Jiaman Li¹, Alexander Clegg², Roozbeh Mottaghi², Jiajun Wu¹, Xavier Puig^{2†}, C. Karen Liu^{1†}
¹Stanford University, ²FAIR, Meta

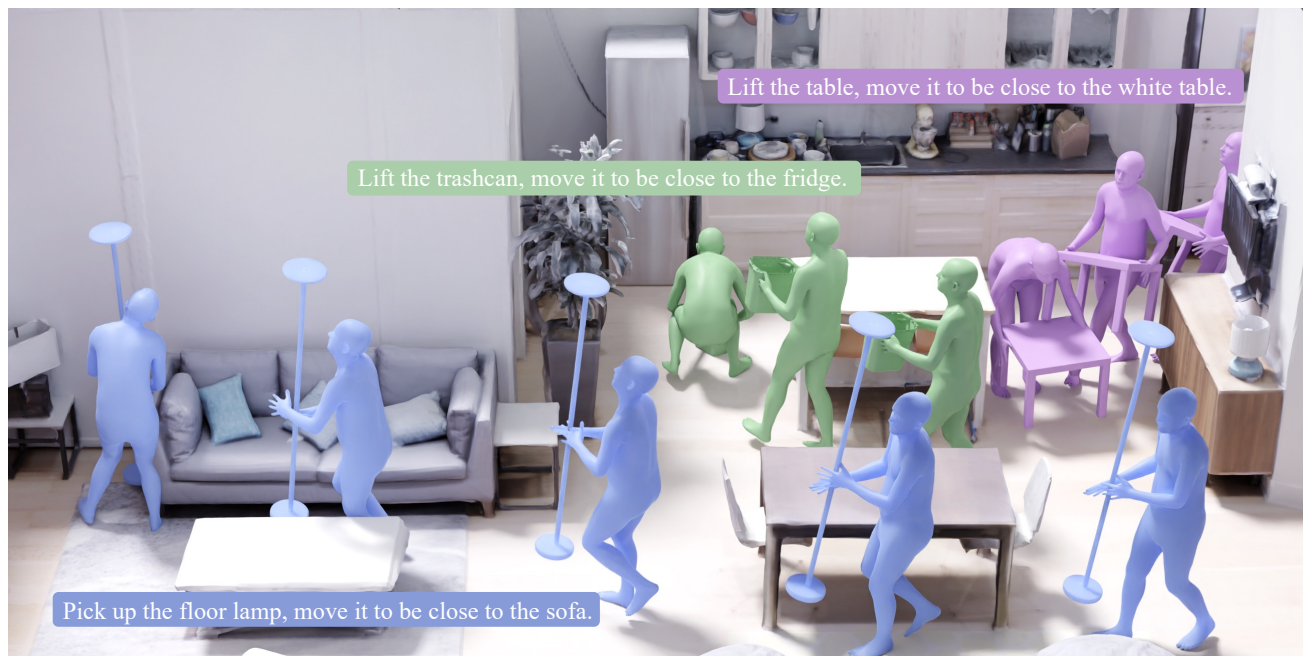


Figure 1. Given an initial object and human state, a language description, and sparse object waypoints in a 3D scene, CHOIS generates synchronized object motion and human motion at the same time.

Abstract

Synthesizing semantic-aware, long-horizon, human-object interaction is critical to simulate realistic human behaviors. In this work, we address the challenging problem of generating synchronized object motion and human motion guided by language descriptions in 3D scenes. We propose Controllable Human-Object Interaction Synthesis (CHOIS), an approach that generates object motion and human motion simultaneously using a conditional diffusion model given a language description, initial object and human states, and sparse object waypoints. While language descriptions inform style and intent, waypoints ground the motion in the scene and can be effectively extracted using high-level planning methods. Naively applying a diffusion model fails to predict object motion aligned with the input waypoints and cannot ensure the realism of interactions that require precise hand-object contact and appropriate contact grounded

by the floor. To overcome these problems, we introduce an object geometry loss as additional supervision to improve the matching between generated object motion and input object waypoints. In addition, we design guidance terms to enforce contact constraints during the sampling process of the trained diffusion model.

1. Introduction

Synthesizing human behaviors in 3D environments is critical for various applications in computer graphics, embodied AI, and robotics. Humans effortlessly navigate and engage within their surroundings, performing a plethora of tasks routinely. For example, drawing a chair closer to a desk to create a workspace, adjusting a floor lamp to cast the perfect glow, or neatly storing a suitcase. Each of these tasks requires precise coordination between the human, the object, and the surroundings. These tasks are also deeply rooted in purpose. Language serves as a powerful tool to articulate and convey these intentions. Synthesizing realistic human and

[†] indicates equal contribution.

object motion guided by language and scene context is the cornerstone of building an advanced AI systems that simulate continuous human behaviors in diverse 3D environments.

While some existing works study the problem of human-scene interaction [18], they are constrained to scenarios with static objects such as sitting on a chair, neglecting the highly dynamic interactions happening frequently in daily life. Recent advancements have been made in modeling dynamic human-object interactions, yet these approaches focus solely on smaller objects [13, 29] or lack the ability to manipulate diverse objects [19, 59]. Manipulating diverse objects of larger size has been explored in recent work [28, 53, 60]. However, these approaches rely on sequences of past interaction states or complete sequences of object motion, and are incapable of synthesizing both object motion and human motion from initial states alone. In this work, we aim to advance the field by focusing on synthesizing realistic interactions involving diverse objects of larger size from language and initial states.

Generating continuous human-object interactions from language descriptions within 3D scenes poses several challenges. First, we need to generate object and human motion which is realistic and synchronized. The human hands should maintain appropriate contact with objects during interaction and object motion should maintain a causal relationship to human actions. Second, 3D scenes are often cluttered with numerous objects, constraining the space of feasible motion trajectories. Thus, it is essential for interaction synthesis to accommodate for environment clutter, rather than operating under the assumption of an empty scene.

In this work, we focus on the key problem of synthesizing human-object interactions in 3D environments from natural language commands, generating object motion and human motion guided by language and sparse object waypoints. Starting with a language description outlining the desired human actions, a set of waypoints extracted from the environment, and an initial object and human state, our goal is to generate motions for both humans and objects. These motions should align with the directives specified in the language input, while also conforming to the environmental constraints defined by waypoint conditions derived from 3D scene geometry.

To achieve this, we employ a conditional diffusion model to generate synchronized object and human motion simultaneously, conditioned on language descriptions, initial states, and sparse object waypoints. To improve the accuracy of the predicted object motion, we incorporate an object geometry loss during training. In addition, we devise guidance terms applied during the sampling process to improve the realism of the generated interaction. Furthermore, we demonstrate the effectiveness of our learned interaction synthesis module within a system that produces continuous realistic and context-aware interactions given language descriptions and

3D scenes.

To summarize, our work makes the following contributions. First, we identify that the combination of language and object waypoints provides precise and expressive information for human-object interaction synthesis. We show that object waypoints do not need to be dense or precise, which allows us to utilize existing path planning algorithms to generate sparse waypoints which represent long-horizon interactions in complex scenarios. Second, based on this finding, we devise a method that synthesizes human-object interaction guided by language and sparse waypoints of the object, using a conditional diffusion model. We demonstrate that our approach synthesizes realistic interactions on FullBody-Manipulation dataset [28]. In addition, the learned model can generalize to novel objects in 3D-FUTURE dataset [11]. Third, we integrate our method into a pipeline that synthesizes long-horizon environment-aware human-object interactions from 3D scenes and language input.

2. Related Work

Motion Synthesis from Language. With the development of large-scale high-quality motion capture datasets like AMASS [30], there has been a growing interest in generative human motion modeling. BABEL [39] and HumanML3D [14] further introduce action labels and language descriptions to enrich the mocap dataset, enabling the development of action-conditioned motion synthesis [36] and text-conditioned motion synthesis [14, 37, 49]. Prior work has shown that VAE formulation is effective in generating diverse human motion from text [14, 15]. Recently, with the success of the diffusion model in this domain [2, 6, 23, 27, 28, 40, 43, 44, 51, 61, 66], extensive work has explored generating motion from text using conditioning [8, 24, 50, 63]. In this work, we also take language descriptions as input to guide our generation. Instead of synthesizing human motion alone, we generate both object motion and human motion conditioned on the text.

Motion Synthesis in 3D Scenes. With the advent of paired scene-motion data [1, 16, 17, 56, 69] and paired object-motion data [18, 64], approaches [1, 18, 25, 54, 55, 64] have been developed to generate human interactions such as sitting on a chair and reaching a target position in 3D scenes. To populate human-object interactions without training on paired scene-motion data, path planning algorithms have been deployed to generate collision-free paths which then guide the human motion generation [18, 33, 65, 67]. Another line of work leverages reinforcement learning frameworks to train scene-aware policies for synthesizing navigation and interaction motions in static 3D scenes [26, 58]. In this work, instead of focusing on static scenes or objects, we synthesize interactions with dynamic objects. Also, inspired by approaches that decompose scene-aware motion generation

into path planning and goal-guided generation phases, we design an interaction synthesis module conditioned on sparse object waypoints that can be effectively integrated into a scene-aware synthesis pipeline.

Interaction Synthesis. The field of modeling dynamic human-object interactions has largely focused on hand motion synthesis [7, 62, 68]. Recently, with the advent of full-body motion datasets with hand-object interactions [10, 47], models [48, 57] have been developed to synthesize full-body motions preceding object grasping. Some recent studies predict object motion based on human movements [35], and others [4, 13, 29] have taken this further by synthesizing both body and hand motion, subsequently applying optimization to predict object motion. However, these approaches focus on smaller objects where hand motion is the primary focus. In terms of manipulating larger objects, some methods train reinforcement learning policies to synthesize box lifting and moving behaviors [19, 32, 59], yet these models struggle to generalize to manipulation of diverse objects. Based on paired human-object motion data [3, 28, 53], recent works predict interactions from a sequence of past interaction states [53, 60] or an object motion sequence [28], incapable of synthesizing interactions in 3D scenes solely from initial states. In this work, we generate synchronized object and human motion conditioned on sparse object waypoints, serving to ground the resulting trajectories in 3D scenes.

3. Method

Our goal is to generate synchronized object and human motion, conditioned on a language description, object geometry, initial object and human states, and sparse object waypoints. Two primary challenges arise in this context: first, modeling the complexity of synchronized object and human motion while also respecting the sparse condition signals; and second, ensuring the realism of contact between the human and object. To tackle the generation problem of complex interactions, we employ a conditional diffusion model to generate object motion and human motion at the same time. However, naively learning a conditional diffusion model to generate both object motion and human motion cannot ensure the precise contact between hand and object and the realism of the interaction. Thus, we incorporate several constraints as guidance during the sampling process of our trained diffusion model. We illustrate our approach in Figure 2.

3.1. Data Representation

Object and Human Motion Representation. We denote the human motion as $\mathbf{X} \in \mathbb{R}^{T \times D}$, where T and D represent the time steps and dimension of the human pose. \mathbf{X}_t , corresponding to the human pose at frame t , consists of global joint positions and 6D continuous rotations [70]. We adopt the widely used parametric human model, SMPL-X [34]

to reconstruct the human mesh from the pose and shape parameters. To represent the object motion, we use two components: the global 3D position and the relative rotation. The global position is represented by the centroid of the object, while the relative rotation, denoted as \mathbf{R}_{rel} at frame t , is expressed with respect to the input object’s geometry \mathbf{V} such that $\mathbf{V}_t = \mathbf{R}_{\text{rel}}\mathbf{V}$, where \mathbf{V}_t represent the vertices of object at frame t . We denote the object motion by $\mathbf{O} \in \mathbb{R}^{T \times 12}$.

Object Geometry Representation. We represent the object geometry using the Basis Point Set (BPS) representation [38]. Following prior work [28], we begin by sampling a set of basis points from a sphere with a 1-meter radius. Subsequently, for each sampled point, we calculate the minimum Euclidean distance to the nearest point on the object’s mesh. Alongside this, we record the directional vectors from the basis points to their nearest neighbors. The resulting BPS representation is denoted as $\mathbf{G} \in \mathbb{R}^{1024 \times 3}$, representing 1024 sampled points each with a 3-dimensional vector indicating their spatial relationship to the object’s surface.

Input Condition Representation. We first use an MLP to project the object BPS representation \mathbf{G} to a low-dimensional vector which is then broadcasted to each frame denoted as $\hat{\mathbf{G}} \in \mathbb{R}^{T \times 256}$ following [28]. We then adopt a masked motion data representation denoted as $\mathbf{S} \in \mathbb{R}^{T \times (12+D)}$ to represent the initial states and waypoint conditions. The initial state contains the human pose and object pose at the first frame. The waypoint conditions consist of a series of 2D object positions for every 30 frames, and a 3D object position at the final frame. The remainder of \mathbf{S} is padded with zeros. The encoded object geometry vector and the masked motion condition vector are then concatenated, serving as part of the input for our denoising network. For effectively integrating language conditions as input, we utilize CLIP [41] as a text encoder to extract language embeddings.

3.2. Interaction Synthesis Model

Conditional Diffusion Model. In our framework, we utilize a conditional diffusion model [21] to generate synchronized object and human motion. To improve the realism of hand-object interaction, our model also predicts contact labels $\mathbf{H} \in \mathbb{R}^{T \times 2}$ for both the left and right hands. These predicted contact labels play a crucial role in guiding the sampling process, ensuring more accurate and realistic hand-object contacts in the generated motion sequence. The complete data representation in our model is denoted as $\tau = \{\mathbf{X}, \mathbf{O}, \mathbf{H}\}$, encapsulating motion and contact data.

The conditional signals of our model, denoted as \mathbf{c} , include initial states, sparse object waypoints, the object BPS representation, and language descriptions. The diffusion model consists of a forward diffusion process that progressively adds noise to the clean data τ_0 and a reverse diffusion process which is trained to reverse this process. The forward

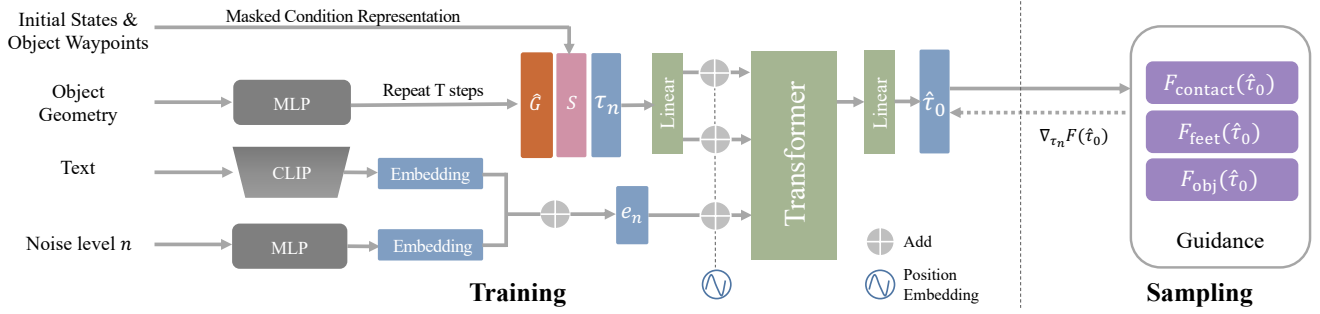


Figure 2. **Method Overview.** Given an object geometry, we use the BPS representation to encode the geometry and an MLP to project the features into a low-dimensional vector. This feature vector is concatenated with masked pose states to form conditions for the denoising network. During sampling, we use analytical functions to compute gradients and perturb the generation to satisfy our defined constraints.

diffusion process introduces noise for N steps formulated using a Markov chain,

$$q(\tau_n | \tau_{n-1}) := \mathcal{N}(\tau_n; \sqrt{1 - \beta_n} \tau_{n-1}, \beta_n \mathbf{I}), \quad (1)$$

$$q(\tau_{1:N} | \tau_0) := \prod_{n=1}^N q(\tau_n | \tau_{n-1}), \quad (2)$$

where β_n represents a fixed variance schedule and \mathbf{I} is an identity matrix. Our goal is to learn a model p_θ to reverse the forward diffusion process,

$$p_\theta(\tau_{n-1} | \tau_n, \mathbf{c}) := \mathcal{N}(\tau_{n-1}; \mu_\theta(\tau_n, n, \mathbf{c}), \Sigma_n), \quad (3)$$

where μ_θ denotes the predicted mean and Σ_n is a fixed variance. Learning the mean can be re-parameterized as learning to predict the clean data representation τ_0 . The objective [21] is defined as

$$\mathcal{L} = \mathbb{E}_{\tau_0, n} \|\hat{\tau}_\theta(\mathbf{x}_n, n, \mathbf{c}) - \tau_0\|_1. \quad (4)$$

Model Architecture. We employ a transformer architecture [52] as our denoising network. Our input consists of object geometry conditions $\hat{\mathbf{G}}$, masked motion conditions \mathbf{S} , and noisy data representation τ_n at noise level n . The input is projected to a sequence of feature vectors using a linear layer. We employ an MLP to embed the noise level n . Then we combine the noise level embedding and the language embedding to form a single embedding vector denoted as e_n . The embedding vector e_n has the same dimension as these feature vectors and is fed to the transformer along with these vectors. The final prediction $\hat{\tau}_0$ is made by projecting the updated feature vectors of the transformer excluding the time step corresponding to the embedding e_n . The interaction synthesis model is illustrated in Figure 2.

Object Geometry Loss. During the training phase, we incorporate an additional loss to improve the object motion prediction. Utilizing the Basis Point Set (BPS) representation, we initially compute the nearest neighbor points on the object mesh in rest pose for each of the fixed set of points. From these, we sample 100 points out of the 1024 nearest neighbors to capture a rough outline of the object’s

shape. These selected points are defined as $\mathbf{K}_{\text{rest}} \in \mathbb{R}^{100 \times 3}$, representing our selected object vertices at rest pose.

At each time step in our model, the predicted object rotation (converted to relative rotation with respect to the object geometry in rest pose) and position are employed to calculate the corresponding positions of these selected vertices. This is represented by the following equation, where $\hat{\mathbf{R}}_t$ and $\hat{\mathbf{d}}_t$ denote the predicted rotation and translation of the object, and \mathbf{K}_t refers to the ground truth vertices at time step t . The object geometry loss is computed as

$$\mathcal{L}_{\text{obj}} = \sum_{t=1}^T \|\hat{\mathbf{R}}_t \mathbf{K}_{\text{rest}} + \hat{\mathbf{d}}_t - \mathbf{K}_t\|_1. \quad (5)$$

This loss function plays a critical role in guiding the model to accurately predict the transformation of the object.

3.3. Guidance

During the training phase of our interaction synthesis model, there are no explicit contact constraints enforced in the losses. Incorporating loss terms such as hand-object contact loss, and object-floor penetration loss poses a challenge for training. First, these types of loss terms are computationally expensive and would slow down training significantly. Second, introducing more loss terms requires meticulously balancing different losses which usually necessitates re-training models with different settings. Instead, enforcing these constraints during test time is more flexible and makes it easier to select appropriate weights for different terms. Thus, to refine our generated interactions, we propose the application of guidance during the sampling process.

In the diffusion model framework, classifier guidance is commonly applied during test time to control the generation process in order to satisfy specific objectives or constraints. A typical approach to applying classifier guidance [9] is to perturb the noisy predicted mean at each denoising step. This is formulated as $\tilde{\mu} = \mu - \alpha \Sigma_n \nabla_{\mu} F(\mu)$, where μ denotes the predicted mean at denoising step n defined by Equation 3. F represents a learned or analytical function that determines how much the predicted mean should be penalized and α represents the strength of the perturbation.

This guidance computes the gradient with respect to the noisy mean, requiring F to be trained on noisy data or a deterministic function designed for noisy data. Another approach is reconstruction guidance [22], which has proven to be effective for controlling the generation process in prior work [24, 25, 42]. Instead of perturbing the noisy mean, it perturbs the predicted clean data representation $\hat{\tau}_0$ using the gradient with respect to the noisy input data representation τ_n . The process is formally represented as

$$\tilde{\tau}_0 = \hat{\tau}_0 - \alpha \Sigma_n \nabla_{\tau_n} F(\hat{\tau}_0). \quad (6)$$

In this work, we leverage reconstruction guidance [22] in the sampling process as we empirically found it to be more stable. We define multiple analytical functions as guidance terms which we will introduce in the following sections.

Hand Object Contact Guidance. We have implemented a specialized contact guidance function to improve the hand-object contact accuracy for frames generated by our model. This function is specifically designed to address cases where a noticeable distance exists between the hands and the object, thereby improving the realism and precision of the interaction. The contact guidance function is defined as follows:

$$F_{\text{contact}} = M_l \|J_l - V_l\|_1 + M_r \|J_r - V_r\|_1. \quad (7)$$

In this equation, M_l and M_r are binary masks for the left and right hand, respectively. These masks are derived from the predicted contact labels H , with $M_l, M_r \in \mathbb{R}^{T \times 1}$ and are defined as $M_l, M_r = (H > 0.95)$. This thresholding identifies frames where contact is likely to occur. $J_l, J_r \in \mathbb{R}^{T \times 3}$ represent the positions of the left and right hands. Meanwhile, $V_l, V_r \in \mathbb{R}^{T \times 3}$ denotes the nearest neighbor points on the object mesh to the respective hand positions.

Feet-Floor Contact Guidance. When generating joint positions and rotations, our model operates without awareness of the body’s shape. Consequently, using the SMPL-X model [34] with predicted root positions, joint rotations, and a test subject’s specific body shape parameters to reconstruct the human mesh can sometimes lead to scenarios where the feet do not touch the floor. To rectify this, we implement a guidance term that encourages realistic feet-floor contact.

The joint positions of the left and right toes are represented as J_l and J_r , respectively. We identify the supporting foot in each frame by comparing the z components of these two joints at each frame. We also introduce a threshold height $h = 0.02$ meters, which is determined from the analysis of foot height in the ground truth motion. The guidance term is defined as follows:

$$F_{\text{feet}} = \|\min(J_l^z, J_r^z) - h\|_2. \quad (8)$$

This function computes the norm of the vertical difference between the lowest point of either toe and the threshold height h .

Object-Floor Penetration Guidance. To address the issue of generated object states potentially penetrating the floor, we integrate an additional guidance function into the sampling process. Given that our floor is positioned at the plane where $z = 0$, we define the guidance term as follows:

$$F_{\text{obj}} = \|\min(V^z, 0)\|_1, \quad (9)$$

where V^z represents the z-coordinate of the object vertices.

During the inference phase, we apply multiple guidance concurrently defined as follows,

$$F_{\text{all}} = \lambda_1 F_{\text{contact}} + \lambda_2 F_{\text{feet}} + \lambda_3 F_{\text{obj}}, \quad (10)$$

where $\lambda_1, \lambda_2, \lambda_3$ denote the loss weights for different terms. We apply the guidance in the last 10 denoising steps only since the prediction in the early steps is extremely noisy.

4. Experiments

We first introduce the datasets and evaluation metrics. Then we show comparisons of our proposed approach against the baselines. We further conduct a human perceptual study to complement our evaluation and ablation study to verify the effectiveness of our proposed guidance terms. Moreover, we demonstrate an application that generates long-term interactions conditioned on object waypoints extracted from 3D scenes.

4.1. Datasets

The FullBodyManipulation dataset [28] consists of 10 hours of high-quality, paired object and human motion, including interaction with 15 different objects. However, our study does not encompass the generation of motion for articulated objects, leading us to exclude sequences related to two such objects (vacuum and mop). We employ this dataset both for training our interaction model and for evaluating the generated results. The training set comprises 15 subjects, with an additional 2 subjects designated for testing, adhering to the dataset partitioning used in OMOMO [28].

The 3D-FUTURE dataset [12] includes 3D models of various furniture items. From this dataset, we select 17 objects representing diverse types (such as chairs, tables, floor lamps, and boxes). This dataset serves to test our model’s ability to generalize to objects it has not previously encountered. Given that the 3D-FUTURE dataset only includes 3D models, we integrate object position data from the testing set of the FullBodyManipulation dataset [28] for evaluation.

4.2. Evaluation Metrics

Condition Matching Metric: This metric calculates the Euclidean distance between the predicted and input object waypoints. It includes the start object position error (T_s), end object position error (T_e), and waypoint errors (T_{xy}), all measured in centimeters (cm).

Method	Condition Matching			Human Motion		Interaction					GT Difference			
	$T_s \downarrow$	$T_e \downarrow$	$T_{xy} \downarrow$	$H_{feet} \downarrow$	FS \downarrow	$C_{prec} \uparrow$	$C_{rec} \uparrow$	$C_{F_1} \uparrow$	$C_{\%} \uparrow$	$P_{hand} \downarrow$	MPJPE \downarrow	$T_{root} \downarrow$	$T_{obj} \downarrow$	$O_{obj} \downarrow$
OMOMO [28]	0	0	0	7.21	0.41	0.68	0.56	0.57	0.54	0.51	21.73	36.62	17.12	1.21
CHOIS w/o L_{obj}	5.76	14.16	8.44	6.55	0.40	0.75	0.50	0.55	0.43	0.66	14.34	21.97	15.53	0.98
CHOIS w/o F_{all}	1.75	6.61	2.69	6.64	0.38	0.78	0.49	0.55	0.41	0.65	15.23	24.13	11.51	0.99
CHOIS (ours)	1.71	6.31	2.87	4.20	0.35	0.80	0.64	0.67	0.54	0.59	15.30	24.43	12.53	0.99

Table 1. **Interaction synthesis** on the FullBodyManipulation dataset [28].

	Condition Matching			Human Motion		Interaction	
	$T_s \downarrow$	$T_e \downarrow$	$T_{xy} \downarrow$	$H_{feet} \downarrow$	FS \downarrow	$C_{\%} \uparrow$	$P_{hand} \downarrow$
OMOMO [28]	0	0	0	6.39	0.43	0.40	0.10
CHOIS w/o L_{obj}	6.70	13.73	7.99	5.68	0.41	0.36	0.30
CHOIS w/o F_{all}	5.75	7.96	2.68	5.84	0.39	0.33	0.26
CHOIS (ours)	4.12	7.35	2.92	3.75	0.38	0.48	0.15

Table 2. **Interaction synthesis** on the 3D-FUTURE dataset [11].

Human Motion Quality Metric: This metric encompasses the foot sliding score (FS) and foot heights (H_{feet}). FS is the weighted average of accumulated translation in the xy plane, following prior work [20], measured in centimeters (cm). H_{feet} assesses the height of the feet, also in centimeters.

Interaction Quality Metric: This metric assesses the accuracy of hand-object interactions, encompassing both contacts and penetrations. For contact accuracy, it employs precision (C_{prec}), recall (C_{rec}), and F1 score (C_{F_1}) metrics following prior work [28]. Additionally, it includes contact percentage ($C_{\%}$), determined by the proportion of frames where contact is detected. To compute the penetration score (P_{hand}), each vertex of the hand V_i is used to query the precomputed object’s Signed Distance Field (SDF). This process yields a corresponding distance value d_i for each vertex. The penetration score is then derived by computing the average of the negative distance values (representing penetration), formalized as $\frac{1}{n} \sum_{i=1}^n |\min(d_i, 0)|$, measured in centimeters (cm).

Ground Truth (GT) Difference Metric: This metric measures the deviation of generated results from the ground truth motion. It comprises the mean per-joint position error (MPJPE), translation error of the root joint (T_{root}), and object position error (T_{obj}), all computed using the Euclidean distance between the predicted and actual ground truth positions in centimeters (cm). Additionally, this metric includes the root joint orientation error (O_{root}) and the object orientation error (O_{obj}). These errors are calculated with the Frobenius norm of the rotational difference, formulated as $\|\mathbf{R}_{pred} \mathbf{R}_{gt}^{-1} - \mathbf{I}\|_2$ where \mathbf{R}_{pred} and \mathbf{R}_{gt} represent the predicted and ground truth rotation matrices respectively.

4.3. Results

Baselines. As there is no prior work presenting a solution for our task, we adapt the most related work, OMOMO [28], to our problem setting in order to evaluate against a base-

line. This method was designed for synthesizing human motion from a provided object motion trajectory. Since OMOMO [28] requires a sequence of object states to generate full-body human poses, we implement a linear interpolation strategy for the object positions. This interpolation is based on the given start and end positions of the object, as well as predefined waypoints in the xy-plane. We also maintain a consistent object rotation, using the orientation from the initial frame throughout the entire sequence. Additionally, we evaluate our approach CHOIS against two ablations: CHOIS w/o L_{obj} and CHOIS w/o F_{all} . CHOIS w/o L_{obj} is trained as a conditional diffusion model but does not include an additional object geometry loss. This variant allows us to understand the baseline performance of the diffusion model in a straightforward setup. In contrast, CHOIS w/o F_{all} incorporates the object geometry loss in its training process but operates without guidance during inference. This approach lets us explore the effectiveness of object geometry loss during training while assessing the model’s capability in the absence of guidance.

Results on the FullBodyManipulation Dataset. We evaluate our approach using objects from the FullBodyManipulation dataset [28] as shown in Table 1. Introducing object geometry loss notably improves the condition matching metric. Furthermore, adding guidance during inference leads to better contact accuracy, reduced hand-object penetration, and less foot floating. Note that OMOMO [28] has zero deviation from the input object trajectory since it only predicts human motion and does not change the object motion input. We also showcase qualitative comparisons in Figure 3. Note that OMOMO’s object motion is updated via linear interpolation and thus cannot follow the text prompt (row 2, lifting the table above the head).

Results on the 3D-FUTURE Dataset. To test our model’s ability to generalize to new objects, we conduct evaluations using the 3D-FUTURE dataset [11]. As shown in Table 2, our proposed method outperforms the baseline and the two ablations. We also provide qualitative results in Figure 3.

Human Perceptual Study. We conduct two human perceptual studies to further complement the evaluation of our approach. The first study assesses the consistency between the generated interactions and the text input. The second study evaluates the overall quality of these generated interactions. For each of these studies, we generate 100 sequences

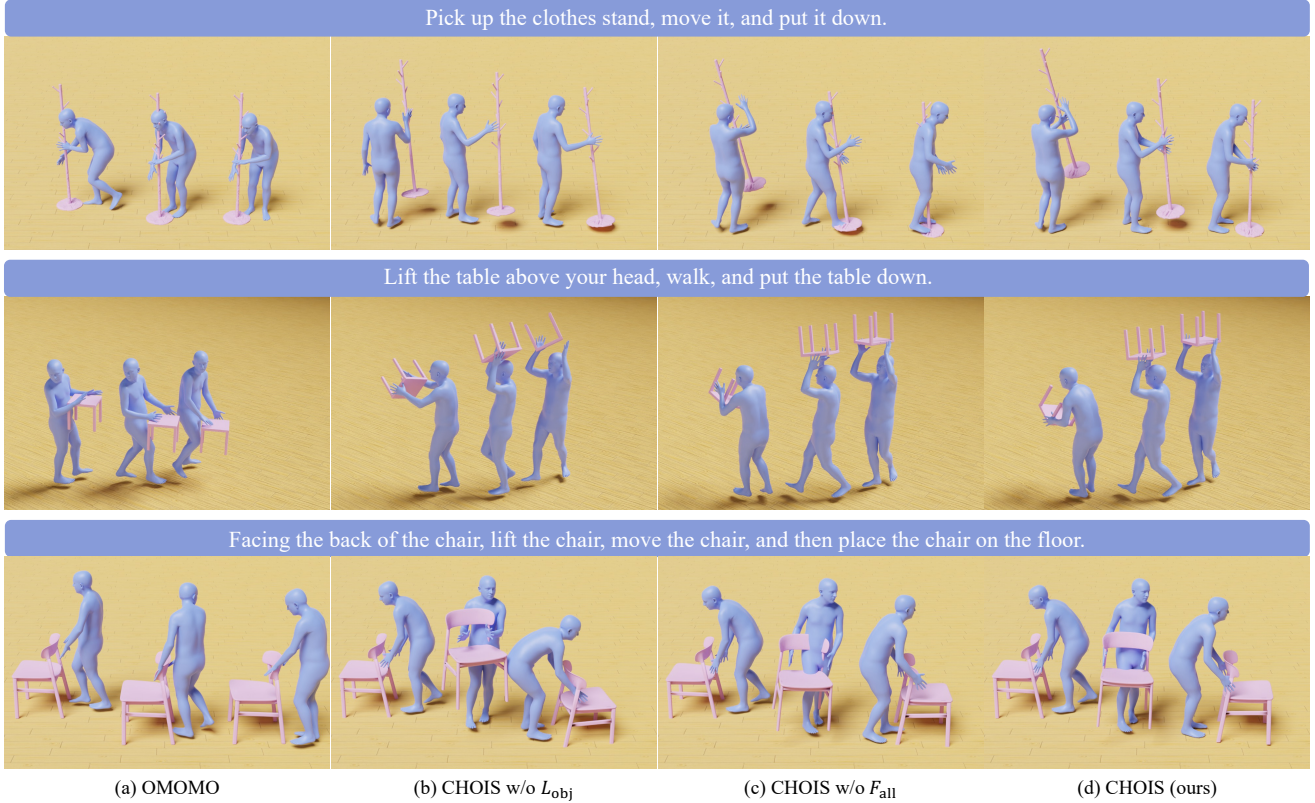


Figure 3. **Qualitative results.** The first two rows show the results on the FullBodyManipulation dataset [28], and the last row shows the results on the 3D-FUTURE dataset [11].

Method	Condition Matching			Human Motion			Interaction				GT Difference			
	$T_s \downarrow$	$T_e \downarrow$	$T_{xy} \downarrow$	$H_{feet} \downarrow$	FS \downarrow	$C_{prec} \uparrow$	$C_{rec} \uparrow$	$C_{F1} \uparrow$	$C\% \uparrow$	$P_{hand} \downarrow$	MPJPE \downarrow	$T_{root} \downarrow$	$T_{obj} \downarrow$	$O_{obj} \downarrow$
CHOIS w/o $F_{contact}$	1.70	6.42	2.70	3.93	0.32	0.78	0.49	0.55	0.41	0.65	15.41	23.63	11.44	0.99
CHOIS w/o F_{feet}	1.72	6.34	2.90	6.65	0.39	0.81	0.64	0.66	0.54	0.58	15.44	25.09	13.31	0.99
CHOIS w/o F_{all}	1.75	6.61	2.69	6.64	0.38	0.78	0.49	0.55	0.41	0.65	15.23	24.13	11.51	0.99
CHOIS (ours)	1.71	6.31	2.87	4.20	0.35	0.80	0.64	0.67	0.54	0.59	15.30	24.43	12.53	0.99

Table 3. **Ablation study** on the FullBodyManipulation dataset [28]. We measure the effect of different guidance terms in the human and object motion generation.

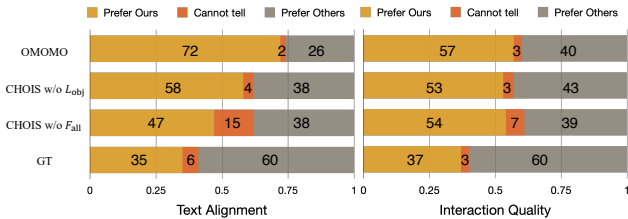


Figure 4. **Results of human perceptual studies.** The numbers shown in the chart represent the percentage (%).

using each method, including our CHOIS, the baseline, our ablations, and the ground truth. This results in a set of 400 pairs. We employ Amazon Mechanical Turk (AMT) for evaluation. Each sequence pair is reviewed by 10 different AMT workers. The results are illustrated in Figure 4. Given that OMOMO [28] generates human motions based solely on interpolated object states and does not incorporate language

	Condition Matching			Human Motion		Interaction	
	$T_s \downarrow$	$T_e \downarrow$	$T_{xy} \downarrow$	$H_{feet} \downarrow$	FS \downarrow	$C\% \uparrow$	$P_{hand} \downarrow$
CHOIS w/o F_{all}	1.50	7.19	5.10	6.01	0.43	0.49	0.70
CHOIS	2.22	9.94	5.73	4.57	0.46	0.63	0.69
CHOIS* w/o F_{all}	6.29	9.39	5.26	4.77	0.39	0.42	0.55
CHOIS*	5.62	12.08	5.95	4.27	0.41	0.65	0.32

Table 4. **Long-term interaction synthesis results** on the FullBodyManipulation [28] and 3D-FUTURE datasets [11]. * represents the results on the 3D-FUTURE dataset.

conditions, our method demonstrates superior performance in aligning with text input. Moreover, our approach shows improvements over the CHOIS w/o L_{obj} , with both CHOIS w/o F_{all} and CHOIS exhibiting comparable proficiency in text alignment. Regarding interaction quality, our method also surpasses all baseline and model ablations.

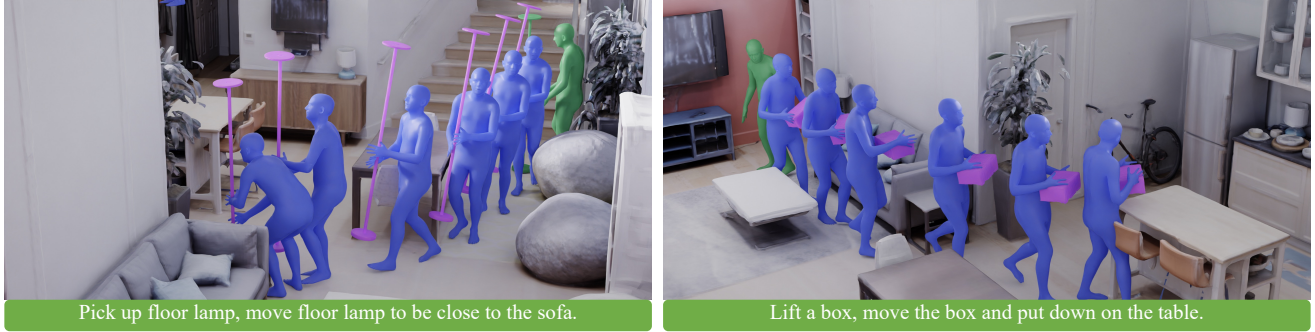


Figure 5. **Long-term interaction synthesis.** Given language descriptions, a 3D scene with semantic labels, and initial human and object states, we synthesize long-term human-object interactions. The initial state is shown in green.



Figure 6. **Results of interaction synthesis** using the same text input but different waypoints. The initial state is in green.

4.4. Ablation Study

We conduct an ablation study to validate the effectiveness of our proposed guidance terms. As shown in Table 3, our hand-object contact guidance and feet-floor contact guidance are both critical. Without the hand-object contact guidance, the contact percentage degrades obviously. Without the feet-floor contact guidance, the height of the feet increases indicating there exists severe foot floating issues. We are not ablating object-floor penetration guidance as object-floor penetration issues are not common and this term is primarily designed for preventing penetration artifacts in qualitative results.

4.5. Application

This section presents a practical application of our method, enabling the synthesis of human-object interactions within 3D scenes, driven by language descriptions. We utilize 3D scenes from the Replica Dataset [45].

The process begins by composing language descriptions that specify the desired interactions, identifying both the objects involved and their intended positions. For example, the language description can be “pull the floor lamp to be close to a shelf”. We also define a set of primitive functions

used to sample target 3D positions from 3D scenes. This set includes functions like sampling points on an object’s surface or near it. GPT-3 [5] is used to extract key information including the interaction object and target objects, and to select the appropriate primitive functions from our predefined function set. Combining the information with the semantic labels of the scene point cloud, we can determine the target 3D positions.

We leverage Habitat [31, 46] to generate collision-free paths within the scene given the start and target object positions. However, as Habitat provides waypoints without corresponding time steps, we need to adapt these to our learned module. We apply heuristics to create waypoints at fixed intervals of 30 frames, which serve as the input conditions for our interaction synthesis model. An example of this application is shown in Figure 5, demonstrating how our learned interaction synthesis model effectively synthesizes human-object motion following a description in a 3D scene. Table 4 includes a quantitative evaluation of the generated motion. In addition, we showcase the results using the same text input but different waypoints in Figure 6, demonstrating the effectiveness of the control using object waypoints.

5. Conclusion

In conclusion, our work addresses the problem of human-object interaction synthesis conditioned on language descriptions and sparse object waypoints. By employing a conditional diffusion model, we successfully generate object and human motions that are not only synchronized but also resonate with given language descriptions. We incorporate object geometry loss during training which significantly improves the performance of object motion generation. We also propose effective guidance terms used during the sampling process which enhance the realism of the generated results. Moreover, we demonstrate that our learned interaction module can be integrated into a pipeline that synthesizes long-term interactions given language and 3D scenes.

Acknowledgments. This work is in part supported by the Stanford Institute for Human-Centered AI (HAI), NSF CCRI #2120095, ONR MURI N00014-22-1-2740, and Meta. Part of the research was done during Jiaman Li’s internship at FAIR, Meta.

References

- [1] Joao Pedro Araujo, Jiaman Li, Karthik Vetrivel, Rishi Agarwal, Deepak Gopinath, Jiajun Wu, Alexander Clegg, and C Karen Liu. Circle: Capture in rich contextual environments. In *Conference on Computer Vision and Pattern Recognition (CVPR)*, 2023. 2
- [2] German Barquero, Sergio Escalera, and Cristina Palmero. Belfusion: Latent diffusion for behavior-driven human motion prediction. In *Proceedings of the IEEE/CVF International Conference on Computer Vision*, pages 2317–2327, 2023. 2
- [3] Bharat Lal Bhatnagar, Xianghui Xie, Ilya A. Petrov, Cristian Sminchisescu, Christian Theobalt, and Gerard Pons-Moll. Behave: Dataset and method for tracking human object interactions. In *Conference on Computer Vision and Pattern Recognition (CVPR)*, pages 15935–15946, 2022. 3
- [4] Jona Braun, Sammy Christen, Muhammed Kocabas, Emre Aksan, and Otmar Hilliges. Physically plausible full-body hand-object interaction synthesis. *arXiv preprint arXiv:2309.07907*, 2023. 3
- [5] Tom Brown, Benjamin Mann, Nick Ryder, Melanie Subbiah, Jared D Kaplan, Prafulla Dhariwal, Arvind Neelakantan, Pranav Shyam, Girish Sastry, Amanda Askell, et al. Language models are few-shot learners. *Advances in neural information processing systems*, 33:1877–1901, 2020. 8
- [6] Xin Chen, Biao Jiang, Wen Liu, Zilong Huang, Bin Fu, Tao Chen, and Gang Yu. Executing your commands via motion diffusion in latent space. In *Proceedings of the IEEE/CVF Conference on Computer Vision and Pattern Recognition*, pages 18000–18010, 2023. 2
- [7] Sammy Christen, Muhammed Kocabas, Emre Aksan, Jemin Hwangbo, Jie Song, and Otmar Hilliges. D-grasp: Physically plausible dynamic grasp synthesis for hand-object interactions. In *Proceedings of the IEEE/CVF Conference on Computer Vision and Pattern Recognition*, pages 20577–20586, 2022. 3
- [8] Rishabh Dabral, Muhammad Hamza Mughal, Vladislav Golyanik, and Christian Theobalt. Mofusion: A framework for denoising-diffusion-based motion synthesis. In *Computer Vision and Pattern Recognition (CVPR)*, 2023. 2
- [9] Prafulla Dhariwal and Alexander Nichol. Diffusion models beat gans on image synthesis. *Advances in neural information processing systems*, 34:8780–8794, 2021. 4
- [10] Zicong Fan, Omid Taheri, Dimitrios Tzionas, Muhammed Kocabas, Manuel Kaufmann, Michael J. Black, and Otmar Hilliges. ARCTIC: A dataset for dexterous bimanual hand-object manipulation. In *Conference on Computer Vision and Pattern Recognition (CVPR)*, 2023. 3
- [11] Huan Fu, Rongfei Jia, Lin Gao, Mingming Gong, Binqiang Zhao, Steve Maybank, and Dacheng Tao. 3d-future: 3d furniture shape with texture. *International Journal of Computer Vision (IJCV)*, 129(12):3313–3337, 2021. 2, 6, 7
- [12] Huan Fu, Rongfei Jia, Lin Gao, Mingming Gong, Binqiang Zhao, Steve Maybank, and Dacheng Tao. 3d-future: 3d furniture shape with texture. *International Journal of Computer Vision*, 129:3313–3337, 2021. 5
- [13] Anindita Ghosh, Rishabh Dabral, Vladislav Golyanik, Christian Theobalt, and Philipp Slusallek. Imos: Intent-driven full-body motion synthesis for human-object interactions. In *Eurographics*, 2023. 2, 3
- [14] Chuan Guo, Shihao Zou, Xinxin Zuo, Sen Wang, Wei Ji, Xingyu Li, and Li Cheng. Generating diverse and natural 3d human motions from text. In *Conference on Computer Vision and Pattern Recognition (CVPR)*, pages 5152–5161, 2022. 2
- [15] Chuan Guo, Xinxin Zuo, Sen Wang, and Li Cheng. Tm2t: Stochastic and tokenized modeling for the reciprocal generation of 3d human motions and texts. In *European Conference on Computer Vision*, pages 580–597. Springer, 2022. 2
- [16] Vladimir Guzov, Aymen Mir, Torsten Sattler, and Gerard Pons-Moll. Human positioning system (hps): 3d human pose estimation and self-localization in large scenes from body-mounted sensors. In *Conference on Computer Vision and Pattern Recognition (CVPR)*, 2021. 2
- [17] Mohamed Hassan, Vasileios Choutas, Dimitrios Tzionas, and Michael J Black. Resolving 3d human pose ambiguities with 3d scene constraints. In *International Conference on Computer Vision (ICCV)*, pages 2282–2292, 2019. 2
- [18] Mohamed Hassan, Duygu Ceylan, Ruben Villegas, Jun Saito, Jimei Yang, Yi Zhou, and Michael Black. Stochastic scene-aware motion prediction. In *International Conference on Computer Vision (ICCV)*, pages 11354–11364, 2021. 2
- [19] Mohamed Hassan, Yunrong Guo, Tingwu Wang, Michael Black, Sanja Fidler, and Xue Bin Peng. Synthesizing physical character-scene interactions. In *SIGGRAPH 2023 Conference Papers*, 2023. 2, 3
- [20] Chengan He, Jun Saito, James Zachary, Holly Rushmeier, and Yi Zhou. Nemf: Neural motion fields for kinematic animation. *Advances in Neural Information Processing Systems (NeurIPS)*, 2022. 6
- [21] Jonathan Ho, Ajay Jain, and Pieter Abbeel. Denoising diffusion probabilistic models. *Advances in Neural Information Processing Systems (NeurIPS)*, 33:6840–6851, 2020. 3, 4
- [22] Jonathan Ho, Tim Salimans, Alexey Gritsenko, William Chan, Mohammad Norouzi, and David J Fleet. Video diffusion models. *arXiv:2204.03458*, 2022. 5
- [23] Siyuan Huang, Zan Wang, Puhao Li, Baoxiong Jia, Tengyu Liu, Yixin Zhu, Wei Liang, and Song-Chun Zhu. Diffusion-based generation, optimization, and planning in 3d scenes. In *Conference on Computer Vision and Pattern Recognition (CVPR)*, 2023. 2
- [24] Korrawe Karunratanakul, Konpat Preechakul, Supasorn Suwajanakorn, and Siyu Tang. Gmd: Controllable human motion synthesis via guided diffusion models. *arXiv preprint arXiv:2305.12577*, 2023. 2, 5
- [25] Nilesh Kulkarni, Davis Remppe, Kyle Genova, Abhijit Kundu, Justin Johnson, David Fouhey, and Leonidas Guibas. Nifty: Neural object interaction fields for guided human motion synthesis. *arXiv preprint arXiv:2307.07511*, 2023. 2, 5

- [26] Jiye Lee and Hanbyul Joo. Locomotion-action-manipulation: Synthesizing human-scene interactions in complex 3d environments. *arXiv preprint arXiv:2301.02667*, 2023. [2](#)
- [27] Jiaman Li, Karen Liu, and Jiajun Wu. Ego-body pose estimation via ego-head pose estimation. In *Proceedings of the IEEE/CVF Conference on Computer Vision and Pattern Recognition*, pages 17142–17151, 2023. [2](#)
- [28] Jiaman Li, Jiajun Wu, and C Karen Liu. Object motion guided human motion synthesis. *ACM Trans. Graph.*, 42(6), 2023. [2](#), [3](#), [5](#), [6](#), [7](#)
- [29] Quanzhou Li, Jingbo Wang, Chen Change Loy, and Bo Dai. Task-oriented human-object interactions generation with implicit neural representations. *arXiv preprint arXiv:2303.13129*, 2023. [2](#), [3](#)
- [30] Naureen Mahmood, Nima Ghorbani, Nikolaus F Troje, Gerard Pons-Moll, and Michael J Black. Amass: Archive of motion capture as surface shapes. In *International Conference on Computer Vision (ICCV)*, pages 5442–5451, 2019. [2](#)
- [31] Manolis Savva*, Abhishek Kadian*, Oleksandr Maksymets*, Yili Zhao, Erik Wijmans, Bhavana Jain, Julian Straub, Jia Liu, Vladlen Koltun, Jitendra Malik, Devi Parikh, and Dhruv Batra. Habitat: A Platform for Embodied AI Research. In *Proceedings of the IEEE/CVF International Conference on Computer Vision (ICCV)*, 2019. [8](#)
- [32] Josh Merel, Saran Tunyasuvunakool, Arun Ahuja, Yuval Tassa, Leonard Hasenclever, Vu Pham, Tom Erez, Greg Wayne, and Nicolas Heess. Catch & carry: reusable neural controllers for vision-guided whole-body tasks. *ACM Transactions on Graphics (TOG)*, 39(4):39–1, 2020. [3](#)
- [33] Aymen Mir, Xavier Puig, Angjoo Kanazawa, and Gerard Pons-Moll. Generating continual human motion in diverse 3d scenes. *arXiv preprint arXiv:2304.02061*, 2023. [2](#)
- [34] Georgios Pavlakos, Vasileios Choutas, Nima Ghorbani, Timo Bolkart, Ahmed A. A. Osman, Dimitrios Tzionas, and Michael J. Black. Expressive body capture: 3d hands, face, and body from a single image. In *Conference on Computer Vision and Pattern Recognition (CVPR)*, pages 10975–10985, 2019. [3](#), [5](#)
- [35] Ilya A Petrov, Riccardo Marin, Julian Chibane, and Gerard Pons-Moll. Object pop-up: Can we infer 3d objects and their poses from human interactions alone? In *Proceedings of the IEEE/CVF Conference on Computer Vision and Pattern Recognition*, pages 4726–4736, 2023. [3](#)
- [36] Mathis Petrovich, Michael J Black, and Gül Varol. Action-conditioned 3d human motion synthesis with transformer vae. In *Proceedings of the IEEE/CVF International Conference on Computer Vision*, pages 10985–10995, 2021. [2](#)
- [37] Mathis Petrovich, Michael J Black, and Gül Varol. Temos: Generating diverse human motions from textual descriptions. In *European Conference on Computer Vision*, pages 480–497. Springer, 2022. [2](#)
- [38] Sergey Prokudin, Christoph Lassner, and Javier Romero. Efficient learning on point clouds with basis point sets. In *International Conference on Computer Vision (ICCV)*, pages 4332–4341, 2019. [3](#)
- [39] Abhinanda R Punnakkal, Arjun Chandrasekaran, Nikos Athanasiou, Alejandra Quiros-Ramirez, and Michael J Black. Babel: Bodies, action and behavior with english labels. In *Conference on Computer Vision and Pattern Recognition (CVPR)*, pages 722–731, 2021. [2](#)
- [40] Sigal Raab, Inbal Leibovitch, Guy Tevet, Moab Arar, Amit H Bermano, and Daniel Cohen-Or. Single motion diffusion. *arXiv preprint arXiv:2302.05905*, 2023. [2](#)
- [41] Alec Radford, Jong Wook Kim, Chris Hallacy, Aditya Ramesh, Gabriel Goh, Sandhini Agarwal, Girish Sastry, Amanda Askell, Pamela Mishkin, Jack Clark, et al. Learning transferable visual models from natural language supervision. In *International conference on machine learning*, pages 8748–8763. PMLR, 2021. [3](#)
- [42] Davis Rempe, Zhengyi Luo, Xue Bin Peng, Ye Yuan, Kris Kitani, Karsten Kreis, Sanja Fidler, and Or Litany. Trace and pace: Controllable pedestrian animation via guided trajectory diffusion. In *Proceedings of the IEEE/CVF Conference on Computer Vision and Pattern Recognition*, pages 13756–13766, 2023. [5](#)
- [43] Yonatan Shafir, Guy Tevet, Roy Kapon, and Amit H Bermano. Human motion diffusion as a generative prior. *arXiv preprint arXiv:2303.01418*, 2023. [2](#)
- [44] Yi Shi, Jingbo Wang, Xuekun Jiang, and Bo Dai. Controllable motion diffusion model. *arXiv preprint arXiv:2306.00416*, 2023. [2](#)
- [45] Julian Straub, Thomas Whelan, Lingni Ma, Yufan Chen, Erik Wijmans, Simon Green, Jakob J Engel, Raul Mur-Artal, Carl Ren, Shobhit Verma, et al. The replica dataset: A digital replica of indoor spaces. *arXiv preprint arXiv:1906.05797*, 2019. [8](#)
- [46] Andrew Szot, Alex Clegg, Eric Undersander, Erik Wijmans, Yili Zhao, John Turner, Noah Maestre, Mustafa Mukadam, Devendra Chaplot, Oleksandr Maksymets, Aaron Gokaslan, Vladimir Vondrus, Sameer Dharur, Franziska Meier, Wojciech Galuba, Angel Chang, Zsolt Kira, Vladlen Koltun, Jitendra Malik, Manolis Savva, and Dhruv Batra. Habitat 2.0: Training home assistants to rearrange their habitat. In *Advances in Neural Information Processing Systems (NeurIPS)*, 2021. [8](#)
- [47] Omid Taheri, Nima Ghorbani, Michael J. Black, and Dimitrios Tzionas. GRAB: A dataset of whole-body human grasping of objects. In *European Conference on Computer Vision (ECCV)*, 2020. [3](#)
- [48] Omid Taheri, Vasileios Choutas, Michael J Black, and Dimitrios Tzionas. Goal: Generating 4d whole-body motion for hand-object grasping. In *Conference on Computer Vision and Pattern Recognition (CVPR)*, pages 13263–13273, 2022. [3](#)
- [49] Guy Tevet, Brian Gordon, Amir Hertz, Amit H Bermano, and Daniel Cohen-Or. Motionclip: Exposing human motion generation to clip space. In *European Conference on Computer Vision*, pages 358–374. Springer, 2022. [2](#)
- [50] Guy Tevet, Sigal Raab, Brian Gordon, Yonatan Shafir, Amit H Bermano, and Daniel Cohen-Or. Human motion diffusion model. In *International Conference on Learning Representations (ICLR)*, 2023. [2](#)
- [51] Jonathan Tseng, Rodrigo Castellon, and C Karen Liu. Edge: Editable dance generation from music. In *Computer Vision and Pattern Recognition (CVPR)*, 2023. [2](#)
- [52] Ashish Vaswani, Noam Shazeer, Niki Parmar, Jakob Uszkoreit, Llion Jones, Aidan N Gomez, Łukasz Kaiser, and Illia

- Polosukhin. Attention is all you need. In *Advances in Neural Information Processing Systems (NIPS)*, pages 5998–6008, 2017. 4
- [53] Weilin Wan, Lei Yang, Lingjie Liu, Zhuoying Zhang, Ruixing Jia, Yi-King Choi, Jia Pan, Christian Theobalt, Taku Komura, and Wenping Wang. Learn to predict how humans manipulate large-sized objects from interactive motions. *IEEE Robotics and Automation Letters*, 7(2):4702–4709, 2022. 2, 3
- [54] Jiashun Wang, Huazhe Xu, Jingwei Xu, Sifei Liu, and Xiaolong Wang. Synthesizing long-term 3d human motion and interaction in 3d scenes. In *Conference on Computer Vision and Pattern Recognition (CVPR)*, pages 9401–9411, 2021. 2
- [55] Jingbo Wang, Yu Rong, Jingyuan Liu, Sijie Yan, Dahua Lin, and Bo Dai. Towards diverse and natural scene-aware 3d human motion synthesis. In *Conference on Computer Vision and Pattern Recognition (CVPR)*, pages 20460–20469, 2022. 2
- [56] Zan Wang, Yixin Chen, Tengyu Liu, Yixin Zhu, Wei Liang, and Siyuan Huang. Humanise: Language-conditioned human motion generation in 3d scenes. In *Advances in Neural Information Processing Systems (NeurIPS)*, 2022. 2
- [57] Yan Wu, Jiahao Wang, Yan Zhang, Siwei Zhang, Otmar Hilliges, Fisher Yu, and Siyu Tang. Saga: Stochastic whole-body grasping with contact. In *European Conference on Computer Vision (ECCV)*, pages 257–274, 2022. 3
- [58] Zeqi Xiao, Tai Wang, Jingbo Wang, Jinkun Cao, Wenwei Zhang, Bo Dai, Dahua Lin, and Jiangmiao Pang. Unified human-scene interaction via prompted chain-of-contacts. *arXiv preprint arXiv:2309.07918*, 2023. 2
- [59] Zhaoming Xie, Jonathan Tseng, Sebastian Starke, Michiel van de Panne, and C Karen Liu. Hierarchical planning and control for box loco-manipulation. *Symposium on Computer Animation (SCA)*, 2023. 2, 3
- [60] Sirui Xu, Zhengyuan Li, Yu-Xiong Wang, and Liang-Yan Gui. Interdiff: Generating 3d human-object interactions with physics-informed diffusion. In *Proceedings of the IEEE/CVF International Conference on Computer Vision*, pages 14928–14940, 2023. 2, 3
- [61] Ye Yuan, Jiaming Song, Umar Iqbal, Arash Vahdat, and Jan Kautz. Physdiff: Physics-guided human motion diffusion model. In *Proceedings of the IEEE/CVF International Conference on Computer Vision*, pages 16010–16021, 2023. 2
- [62] He Zhang, Yuting Ye, Takaaki Shiratori, and Taku Komura. Manipnet: neural manipulation synthesis with a hand-object spatial representation. *ACM Transactions on Graphics (ToG)*, 40(4):1–14, 2021. 3
- [63] Mingyuan Zhang, Zhongang Cai, Liang Pan, Fangzhou Hong, Xinying Guo, Lei Yang, and Ziwei Liu. Motiondiffuse: Text-driven human motion generation with diffusion model. *arXiv preprint arXiv:2208.15001*, 2022. 2
- [64] Xiaohan Zhang, Bharat Lal Bhatnagar, Sebastian Starke, Vladimir Guzov, and Gerard Pons-Moll. Couch: Towards controllable human-chair interactions. In *European Conference on Computer Vision (ECCV)*, pages 518–535, 2022. 2
- [65] Yan Zhang and Siyu Tang. The wanderings of odysseus in 3d scenes. In *Conference on Computer Vision and Pattern Recognition (CVPR)*, pages 20481–20491, 2022. 2
- [66] Zihan Zhang, Richard Liu, Kfir Aberman, and Rana Hanocka. Tedi: Temporally-entangled diffusion for long-term motion synthesis. *arXiv preprint arXiv:2307.15042*, 2023. 2
- [67] Kaifeng Zhao, Yan Zhang, Shaofei Wang, Thabo Beeler, and Siyu Tang. Synthesizing diverse human motions in 3d indoor scenes. *arXiv preprint arXiv:2305.12411*, 2023. 2
- [68] Juntian Zheng, Qingyuan Zheng, Lixing Fang, Yun Liu, and Li Yi. Cams: Canonicalized manipulation spaces for category-level functional hand-object manipulation synthesis. In *Proceedings of the IEEE/CVF Conference on Computer Vision and Pattern Recognition*, pages 585–594, 2023. 3
- [69] Yang Zheng, Yanchao Yang, Kaichun Mo, Jiaman Li, Tao Yu, Yebin Liu, Karen Liu, and Leonidas Guibas. Gimo: Gaze-informed human motion prediction in context. In *European Conference on Computer Vision (ECCV)*, 2022. 2
- [70] Yi Zhou, Connelly Barnes, Jingwan Lu, Jimei Yang, and Hao Li. On the continuity of rotation representations in neural networks. In *Computer Vision and Pattern Recognition (CVPR)*, 2019. 3